REPORT DOCUMENTATION PAGE

Form Approved OMB NO. 0704-0188

1. REPORT DATE (DD-MM-YYYY)	2. REPORT TYPE	3. DATES COVERED (From - To)
04-01-2011	Final Report	10-Nov-2006 - 30-Jul-2010

4. TITLE AND SUBTITLE
Computational Model for Domain Structure Evolution in Ferroelectrics

5a. CONTRACT NUMBER
W911NF-07-1-0041

5b. GRANT NUMBER

5c. PROGRAM ELEMENT NUMBER
611102

6. AUTHORS
Chad M. Landis

5d. PROJECT NUMBER

5e. TASK NUMBER

5f. WORK UNIT NUMBER

7. PERFORMING ORGANIZATION NAMES AND ADDRESSES
University of Texas at Austin
The University of Texas at Austin
101 East 27th Street
Austin, TX 78712 -1500

8. PERFORMING ORGANIZATION REPORT NUMBER

9. SPONSORING/MONITORING AGENCY NAME(S) AND ADDRESS(ES)
U.S. Army Research Office
P.O. Box 12211
Research Triangle Park, NC 27709-2211

10. SPONSOR/MONITOR'S ACRONYM(S)
ARO

11. SPONSOR/MONITOR'S REPORT NUMBER(S)
52295-MS.1

12. DISTRIBUTION AVAILIBILITY STATEMENT
Approved for Public Release; Distribution Unlimited

13. SUPPLEMENTARY NOTES
The views, opinions and/or findings contained in this report are those of the author(s) and should not contrued as an official Department of the Army position, policy or decision, unless so designated by other documentation.

14. ABSTRACT
The goal of the proposed research is to develop a sound theoretical framework and advanced numerical techniques to simulate the evolution of domain microstructures in ferroelectric materials. Ferroelectric ceramics are presently being used in a broad range of applications including fuel injectors for high efficiency-low emission diesel engines, actuators for active control of helicopter rotor blades and underwater vehicle control surfaces, and ultrasonic rotary inchworm motors with high power and torque densities. Additionally, ferroelectric thin films are used for data

15. SUBJECT TERMS
ferroelectric, fracture, microstructural evolution, phase-field model, finite element modeling

16. SECURITY CLASSIFICATION OF:			17. LIMITATION OF ABSTRACT	15. NUMBER OF PAGES	19a. NAME OF RESPONSIBLE PERSON
a. REPORT	b. ABSTRACT	c. THIS PAGE			Chad Landis
UU	UU	UU	UU		19b. TELEPHONE NUMBER 512-471-4273

Report Title

Computational Model for Domain Structure Evolution in Ferroelectrics

ABSTRACT

The goal of the proposed research is to develop a sound theoretical framework and advanced numerical techniques to simulate the evolution of domain microstructures in ferroelectric materials. Ferroelectric ceramics are presently being used in a broad range of applications including fuel injectors for high efficiency-low emission diesel engines, actuators for active control of helicopter rotor blades and underwater vehicle control surfaces, and ultrasonic rotary inchworm motors with high power and torque densities. Additionally, ferroelectric thin films are used for data storage in non-volatile ferroelectric random access memory (NVFRAM), sensing and actuation in microelectromechanical system (MEMS), and in nonlinear optics. An understanding of microstructural evolution and domain dynamics is necessary for further development of micro/nano-ferroelectric device technology. We intend to develop a combined theoretical and numerical modeling framework in order to investigate the interactions of domain walls with surfaces, charges, dislocations and other types of defects. Such studies will aid in the understanding of device performance and of material failure mechanisms.

Enter List of papers submitted or published that acknowledge ARO support from the start of the project to the date of this printing. List the papers, including journal references, in the following categories:

(a) Papers published in peer-reviewed journals (N/A for none)

W. Li and C.M. Landis, "Phase-field modeling of domain switching near crack tips in single crystal ferroelectrics," Proceedings of the SPIE 6929 (2008) 69290J.

A. Kontsos, W. Li and C.M. Landis, "Computational phase-field modeling of defect interactions in ferroelectrics," Proceedings of the SPIE 7289 (2009) 72890D.

A. Kontsos and C.M. Landis, "Computational modeling of domain wall interactions with dislocations in ferroelectric crystals," International Journal of Solids and Structures 46 (2009) 1491-1498.

D. Carka and C.M. Landis, "On the path-dependence of the J-integral near a stationary crack in an elastic-plastic material," Journal of Applied Mechanics 78 (2011) 011006.

D. Carka, M.E. Mear and C.M. Landis, "The Dirichlet-to-Neumann map for two-dimensional crack problems," Computer Methods in Applied Mechanics and Engineering, in press (2010) doi:10.1016/j.cma.2010.10.016.

Number of Papers published in peer-reviewed journals: 5.00

(b) Papers published in non-peer-reviewed journals (N/A for none)

Received	Paper

TOTAL:

Number of Papers published in non peer-reviewed journals: 0.00

(c) Presentations

C.M. Landis, “Modeling of Domain Wall Defect Interactions in Ferroelectric Single Crystals”, Departmental Seminar, University of Virginia, February 28, 2008.

C.M. Landis, “Continuum Modeling of Defect Interactions in Smart Materials”, Departmental Seminar, Texas A&M University, June 2, 2008.

A. Kontsos and C.M. Landis, “Computational Modeling of Domain Wall Interactions with Dislocations in Ferroelectric Crystals”, ASME IMECE 2008, Boston, MA, November 5, 2008.

C.M. Landis and W. Li, “Phase-field Modeling of Domain Switching near Crack Tips in Single Crystal Ferroelectrics”, ASME IMECE 2008, Boston, MA, November 5, 2008.

C.M. Landis, “Phase-field Modeling of Defect Interactions in Active Materials”, TMS 2009, San Francisco, CA, February 17, 2009.

C.M. Landis, “Domain Wall – Defect Interactions in Ferroelectrics”, Departmental Seminar, University of Nebraska, April 7, 2009.

C.M. Landis and A. Kontsos, “Phase-Field Modeling of Domain Structures in Ferroelectric Thin Films”, 2009 Joint ASCE-ASME-SES Conference on Mechanics and Materials, Blacksburg, VA, June 25, 2009.

C.M. Landis and A. Kontsos, “The Structure of the Paraelectric-Ferroelectric Phase Boundary Interface”, Smart Structures and Materials 2010, San Diego, CA, March 8, 2010.

C.M. Landis and W. Li, “A Finite Deformation Phase-Field Theory of Ferroelectrics”, Smart Structures and Materials 2010, San Diego, CA, March 8, 2010.

C.M. Landis and D. Carka, “On the Path-Dependence of the J-Integral in Elastic-Plastic Materials”, U.S. National Congress on Theoretical and Applied Mechanics 2010, State College, PA, July 1, 2010.

C.M. Landis and W. Li, “Modeling of the Nucleation and Growth of Domain Needles”, ASME 2010 Conference on Smart Materials, Adaptive Structures and Intelligent Systems, Philadelphia, PA, September 29, 2010.

Number of Presentations: 11.00

Non Peer-Reviewed Conference Proceeding publications (other than abstracts):

Received	Paper

TOTAL:

Number of Non Peer-Reviewed Conference Proceeding publications (other than abstracts): 0

Peer-Reviewed Conference Proceeding publications (other than abstracts):

Received	Paper

TOTAL:

Number of Peer-Reviewed Conference Proceeding publications (other than abstracts): 0

(d) Manuscripts

D. Carka, R.M. McMeeking and C.M. Landis, "A note on the path-dependence of the J-integral near a stationary crack in an elastic-plastic material with finite deformation," Journal of Applied Mechanics, submitted (2010).

W. Li and C.M. Landis, "Nucleation and growth of domains near crack tips in single crystal ferroelectrics," Engineering Fracture Mechanics, accepted (2010).

Number of Manuscripts: 2.00

Books

Received	Paper

TOTAL:

Patents Submitted

Patents Awarded

Awards

2008 Thomas J.R. Hughes Young Investigator Award (ASME Applied Mechanics Division)

Graduate Students

NAME	PERCENT_SUPPORTED
Wenyuan Li	0.50
Dorinamaria Carka	0.50
FTE Equivalent:	**1.00**
Total Number:	**2**

Names of Post Doctorates

NAME	PERCENT_SUPPORTED
Antonios Kontsos	0.25
FTE Equivalent:	**0.25**
Total Number:	**1**

Names of Faculty Supported

NAME	PERCENT_SUPPORTED	National Academy Member
Chad M. Landis	0.08	No
FTE Equivalent:	**0.08**	
Total Number:	**1**	

Names of Under Graduate students supported

NAME	PERCENT_SUPPORTED
FTE Equivalent:	
Total Number:	

Student Metrics

This section only applies to graduating undergraduates supported by this agreement in this reporting period

The number of undergraduates funded by this agreement who graduated during this period:	0.00
The number of undergraduates funded by this agreement who graduated during this period with a degree in science, mathematics, engineering, or technology fields:.....	0.00
The number of undergraduates funded by your agreement who graduated during this period and will continue to pursue a graduate or Ph.D. degree in science, mathematics, engineering, or technology fields:.....	0.00
Number of graduating undergraduates who achieved a 3.5 GPA to 4.0 (4.0 max scale):	0.00
Number of graduating undergraduates funded by a DoD funded Center of Excellence grant for Education, Research and Engineering:	0.00
The number of undergraduates funded by your agreement who graduated during this period and intend to work for the Department of Defense	0.00
The number of undergraduates funded by your agreement who graduated during this period and will receive scholarships or fellowships for further studies in science, mathematics, engineering or technology fields:	0.00

Names of Personnel receiving masters degrees

NAME

Total Number:

Names of personnel receiving PHDs

NAME

Total Number:

Names of other research staff

NAME PERCENT_SUPPORTED

FTE Equivalent:

Total Number:

Sub Contractors (DD882)

Inventions (DD882)

Scientific Progress

See Attachment

Technology Transfer

Table of Contents

List of Figures and Appendices

Statement of Problem Studied

Computational Model for Domain Structure Evolution in Ferroelectrics

Final Report

PI: Chad M. Landis
Students: Wenyuan Li and Dorinamaria Carka
Post-doc: Antonios Kontsos

The goal of the proposed research is to develop a sound theoretical framework and advanced numerical techniques to simulate the evolution of domain microstructures in ferroelectric materials. Ferroelectric ceramics are presently being used in a broad range of applications including fuel injectors for high efficiency-low emission diesel engines, actuators for active control of helicopter rotor blades and underwater vehicle control surfaces, and ultrasonic rotary inchworm motors with high power and torque densities. Additionally, ferroelectric thin films are used for data storage in non-volatile ferroelectric random access memory (NVFRAM), sensing and actuation in microelectromechanical system (MEMS), and in nonlinear optics. An understanding of microstructural evolution and domain dynamics is necessary for further development of micro/nano-ferroelectric device technology. We developed a combined theoretical and numerical modeling framework in order to investigate the interactions of domain walls with surfaces, grain boundaries, charges, dislocations and other types of defects. Such studies will aid in the understanding of device performance and of material failure mechanisms.

Summary of Important Results

Theoretical Foundations

Here we review the fundamental governing phase-field equations. Standard index notation is used with summation implied over repeated indices, the overdot represents the first derivative with respect to time, and $,j$ represents partial differentiation with respect to the x_j coordinate direction.

The static equilibrium equations in any arbitrary volume V and its bounding surfaces S yield,

$$\sigma_{ji,j} + b_i = 0 \text{ in } V \tag{1}$$

$$\sigma_{ij} = \sigma_{ji} \text{ in } V \tag{2}$$

$$\sigma_{ji} n_j = t_i \text{ on } S \tag{3}$$

Where σ_{ij} are the Cartesian components of the Cauchy stress, b_i the components of a body force per unit volume, n_i the components of a unit vector normal to a surface element, and t_i the tractions applied to a surface. Under the assumptions of linear kinematics, the strain components ε_{ij} are related to the displacements u_i as

$$\varepsilon_{ij} = \frac{1}{2}\left(u_{i,j} + u_{j,i}\right) \text{in } V \tag{4}$$

The electrical quantities of electric field, E_i, electric potential, ϕ, electric displacement, D_i, volume charge density, q, and surface charge density, ω, are governed by the quasi-static forms of Maxwell's equations. Specifically,

$$D_{i,i} - q = 0 \text{ in } V \tag{5}$$

$$D_i n_i = -\omega \text{ on } S \tag{6}$$

$$E_i = -\phi_{,i} \tag{7}$$

within the phase-field modeling approach the free energy will also be required to depend on an order parameter and its gradient. Mathematically, the order parameter is used to describe the different variant types, i.e. the spontaneous states that are possible. For the case of ferroelectrics, the physically natural order parameter is the electrical

polarization P_i. Note that the relationship between electric field, electric displacement and polarization in matter is given as

$$D_i = P_i + \kappa_0 E_i \tag{8}$$

Here κ_0 is the permittivity of free space. Given that the free energy is permitted to depend on an order parameter, a set of micro-forces are introduced that are work-conjugate to the order parameter and its gradient. The micro-force balance is written as,

$$\xi_{ji,j} + \pi_i + \gamma_i = 0 \tag{9}$$

where we have introduced a micro-force tensor ξ_{ji} such that $\xi_{ji} n_j \dot{P}_i$ represents the power density expended across surfaces, an *internal* micro-force vector π_i such that $\pi_i \dot{P}_i$ is the power density expended by the material internally (this micro-force accounts for dissipation in the material), and an external micro-force vector γ_i such that $\gamma_i \dot{P}_i$ is the power density expended by external sources. After the introduction of the Helmholtz free energy $\psi = \psi\left(\varepsilon_{ij}, D_i, P_i, P_{i,j}\right)$, and an analysis of the second law of thermodynamics, the following constitutive relationships result.

$$\sigma_{ji} = \frac{\partial \psi}{\partial \varepsilon_{ij}},\ E_i = \frac{\partial \psi}{\partial D_i},\ \xi_{ji} = \frac{\partial \psi}{\partial P_{i,j}},\ \text{and}\ \ \pi_i = -\eta_i - \beta_{ij}\dot{P}_j \ \ \text{with } \beta_{ij} \text{ positive definite}, \text{ where}$$

$$\eta_i \equiv \frac{\partial \psi}{\partial P_i} \tag{10}$$

The form of the Helmholtz free energy that is chosen to mimic the behavior of ferroelectric single crystals is,

$$\begin{aligned}
\psi = & \frac{1}{2} a_{ijkl} P_{i,j} P_{k,l} \\
& + \frac{1}{2} \overline{a}_{ij} P_i P_j + \frac{1}{4} \overline{\overline{a}}_{ijkl} P_i P_j P_k P_l + \frac{1}{6} \overline{\overline{\overline{a}}}_{ijklmn} P_i P_j P_k P_l P_m P_n + \frac{1}{8} \overline{\overline{\overline{\overline{a}}}}_{ijklmnrs} P_i P_j P_k P_l P_m P_n P_r P_s \\
& + b_{ijkl} \varepsilon_{ij} P_k P_l + \frac{1}{2} c_{ijkl} \varepsilon_{ij} \varepsilon_{kl} + f_{ijklmn} \varepsilon_{ij} \varepsilon_{kl} P_m P_n + g_{ijklmn} \varepsilon_{ij} P_k P_l P_m P_n \\
& + \frac{1}{2\kappa_0}\left(D_i - P_i\right)\left(D_i - P_i\right)
\end{aligned} \tag{11}$$

The specific values for the constants that are used to model barium titanate are listed in the Appendix. The representation of this free energy contains a few important material parameters to be used for the normalization of the results in this paper, including the spontaneous polarization P_0, the spontaneous strain ε_0, the critical electric field for homogeneous 180° switching E_0, the characteristic stress $\sigma_0 = E_0 P_0 / \varepsilon_0$, and the domain wall length scale l_0.

Numerical Implementation

Solutions to Equations (1)-(11) can be obtained numerically using the finite element method. The nodal degrees of freedom are chosen to include the mechanical displacements, the polarization components, and the electric potential, from which strains, polarization gradients, and electric field values are computed within the elements. The following statement of the principal of virtual work is used to implement the finite element method.

$$\begin{aligned} &\int_V \beta_{ij}\dot{P}_j \delta P_i \, dV + \int_V \left(\sigma_{ji}\delta\varepsilon_{ij} - D_i \delta E_i + \eta_i \delta P_i + \xi_{ji}\delta P_{i,j} \right) dV \\ &\qquad = \int_S \left(b_i \delta u_i - q\delta\varphi + \gamma_i \delta P_i \right) dV + \int_S (t_i \delta u_i - \omega_i \delta\varphi + \xi_{ji} n_j \delta P_i) dS \end{aligned} \tag{12}$$

Standard finite element procedures lead to a set of non-linear algebraic equations for the nodal degrees of freedom, and the solution is obtained using an iterative Newton-Raphson method. Additional details on both the theoretical foundations and the numerical implementation of the phase-field model can be found in References [1-3].

Domain Wall – Dislocation Interactions

Using these theoretical foundations and numerical methods we have studied the interactions of domain walls with defects, including dislocations, crack tips, and free surfaces and interfaces in thin films. Here we present results from applying the phase-field framework to investigate the interactions between domain walls and arrays of dislocations in ferroelectric single crystals. The non-linear finite element method was used to determine equilibrium solutions for the coupled electromechanical interactions between a domain wall and a dislocation array. The numerical simulations demonstrate the effect of the relative size and orientation of dislocations on 180° and 90° domain wall configurations. In addition, results for the pinning strength of dislocations in the case that domain walls move due the application of external electric field and shear stress are computed. The presented numerical results were compared with the findings reported for charged defects and it is shown that non-charged defects, such as dislocations, can

also interact strongly with domain walls, and therefore affect the ferroelectric material behavior.

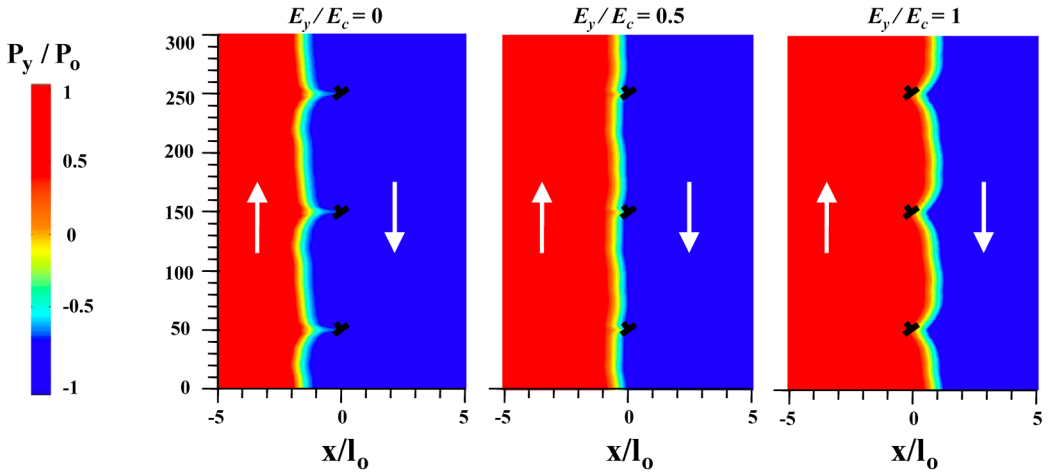

Fig. 1. Polarization distributions in the y-direction near a 180° domain wall interacting with an array of dislocations in the [110] direction. The x-scale is normalized with l_0 and the polarization values with P_0. The solid white arrows designate the direction of the polarization vector. Periodic boundary conditions are enforced on the lines at half the distance $h = 100l_0$ between the dislocations. For $E_y / E_c > 1$ the wall breaks through the dislocation.

Figures 1 and 2 illustrate the types of results produced by our simulations. Upon introducing an array of dislocations, Fig. 1 demonstrates the effects of their interactions with the 180° domain wall configuration. Specifically, P_y polarization distributions are plotted near dislocations with $\mathbf{b} = b[110]$ and $b = 10\varepsilon_0 l_0$. The distance h between the dislocations is equal to $100l_0$. Fig. 1 shows that within the phase-field framework, the domain wall is a diffuse zone where polarization changes smoothly between the adjacent domain states which are marked by solid white arrows. In addition, notice that the wall is kinked with respect to its original straight configuration. In fact, the numerical results reveal that as the dislocation size increases the kinking becomes more pronounced, as expected, indicating stronger interactions between the dislocations and the walls. Domain wall kinking, with a different morphology, has also been reported for domain walls interacting with arrays of point charges. These results demonstrate that the existence of non-charged defects, such as dislocations, cause similar electroelastic interactions in ferroelectrics. It is further observed in Fig. 1 that the equilibrium position of the domain wall, which was initially placed along the y-axis, lies to the left of the arrays of dislocations when no electric field is applied. However, as the applied electrical field increases the domain wall shifts to the right until eventually it breaks through the array of dislocations. In Fig. 1, E_c is the critical value of the electrical field

required to force the domain wall to break though, and for the dislocation size shown it is equal to $0.049E_0$. It is interesting to observe the shape of the kinking and note that the wall always bows towards the dislocation sites. This is a consequence of the details of the electrostatic fields near the defects. Hence, it is apparent that dislocations cause electromechanical interactions that change the shape of a 180° wall, and force the wall to be offset from the array when no external loads are applied.

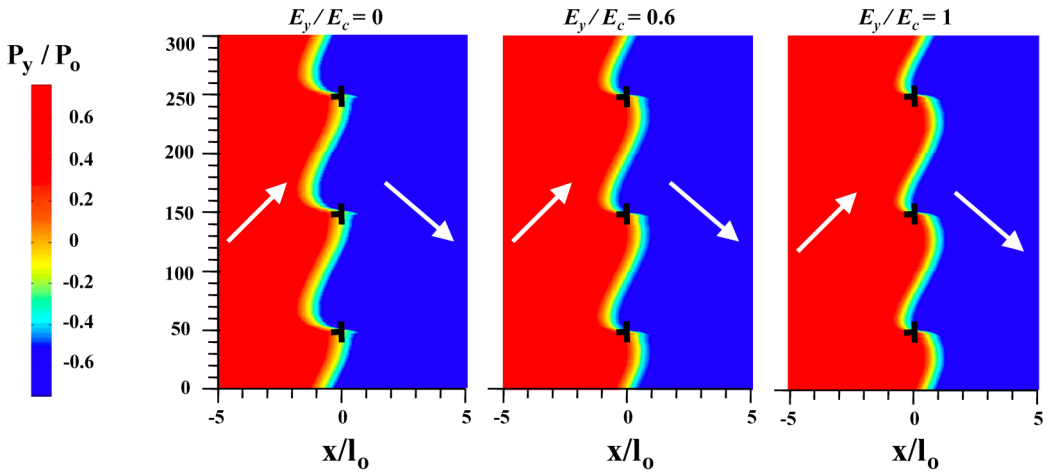

Fig. 2. Polarization distributions in the y-direction near a 90° domain wall interacting with an array of dislocations in the $[\bar{1}10]$ direction having Burger's vectors size $b = 10\varepsilon_0 l_0$ The x-scale is normalized with l_0 and the polarization values with P_0. The solid white arrows designate the direction of the polarization vector. Periodic boundary conditions are enforced on the lines at half the distance $h = 100l_0$ between the dislocations. For $E_y / E_c > 1$ the wall breaks through the dislocation.

Figure 2 shows the effect of applied positive electric field on the configuration of a 90° wall interacting with an array of dislocations in the $[\bar{1}10]$ direction. The electric field values in Fig. 2 are normalized with the critical value $E_c = 0.024E_0$, which causes the wall to break through the dislocations for a Burger's vector size $b = 10\varepsilon_0 l_0$. As seen in this figure, for no applied electric field the electromechanical interactions between the domain wall and the dislocation cause significant kinking of the wall. Compared to the 180° wall, the kinking of the 90° wall is more pronounced for the same dislocation size. The equilibrium position of the 90° wall is centered the array of dislocations and the application of positive electrical field causes the domain wall to shift to the right. When the applied field reaches the critical value E_c, the results shown in Fig. 2 illustrate the equilibrium position just before the wall breaks through the dislocation array. Similar results have been obtained for a 90° wall interacting with [110]-type dislocations. It is further noted that the effects on the domain wall caused by its interaction with the

array of dislocations in the case that electric field is applied are very similar to the corresponding effects caused when only shear stresses are applied. This obervation agress with the case of charged defects interacting with domain walls. Additional details of this study can be found in Reference [2].

Domain Nucleation at a Crack Tip

Next, results for the growth of a new domain from a crack tip during purely electrical loading are reported. To generate the solution for a final equilibrium domain configuration, the domain was nucleated at the crack tip and then allowed to evolve with a non-zero polarization viscosity term (i.e. the first β-term in Equation (12)). The loading is applied by first ramping up a uniform charge load on the top and bottom surfaces with a charging rate of $\beta\dot{\omega}_A / E_0 = 0.1$ to a total charge of $\omega_A / P_0 = 0.16$ in a $60l_0 \times 60l_0$ domain with an electrically impermeable crack half of the way through its midplane. The charge was then fixed at $\omega_A / P_0 = 0.16$ and the domain structure was allowed to evolve until the solution was sufficiently close to the equilibrium configuration, at which point the polarization viscosity term was set to $\beta = 0$ to find the true equilibrium solution. Thereafter additional charge is applied to the surface to a final value of $\omega_A / P_0 = 0.2$ and finally the charge is removed from the surface to return to the initial uncharged state. Note that in order to ensure accuracy of the computations at least five finite element nodes span any domain wall, and the path-independence of the J-integral is verified for all cases of equilibrium. Details of the derivation of the J-integral for this phase-field theory can be found in Reference [3]. If the mesh is too coarse then mesh-pinning of the domains occurs and significant but artificial path-dependence appears at equilibrium in the J-integral. Figure 3 shows contour plots of the y component of the polarization distributions at four different times in the domain evolution. Figure 3 shows that the 90° domain needle is nucleated at the crack tip and propagates through the entire domain until it reaches the charged boundary.

This non-equilibrium propagation of the domain supports the hypothesis that an instability in the equilibrium solution exists at the domain nucleation threshold. Additionally, the equilibrium configurations just prior to the domain nucleation with no domain (not shown in the figure) and the domain configuration shown in Figure 3b both occur at a charge loading level of $\omega_A / P_0 = 0.16$, and are sufficiently distinct from one another. This unstable growth of the domain is in contrast to domain switching zones predicted using phenomenological constitutive laws. The explanation for the discrepancy is that these phase-field simulations assume a defect-free material. In such a material domain walls do not become pinned and are free to move at vanishingly small levels of electromechanical driving force.

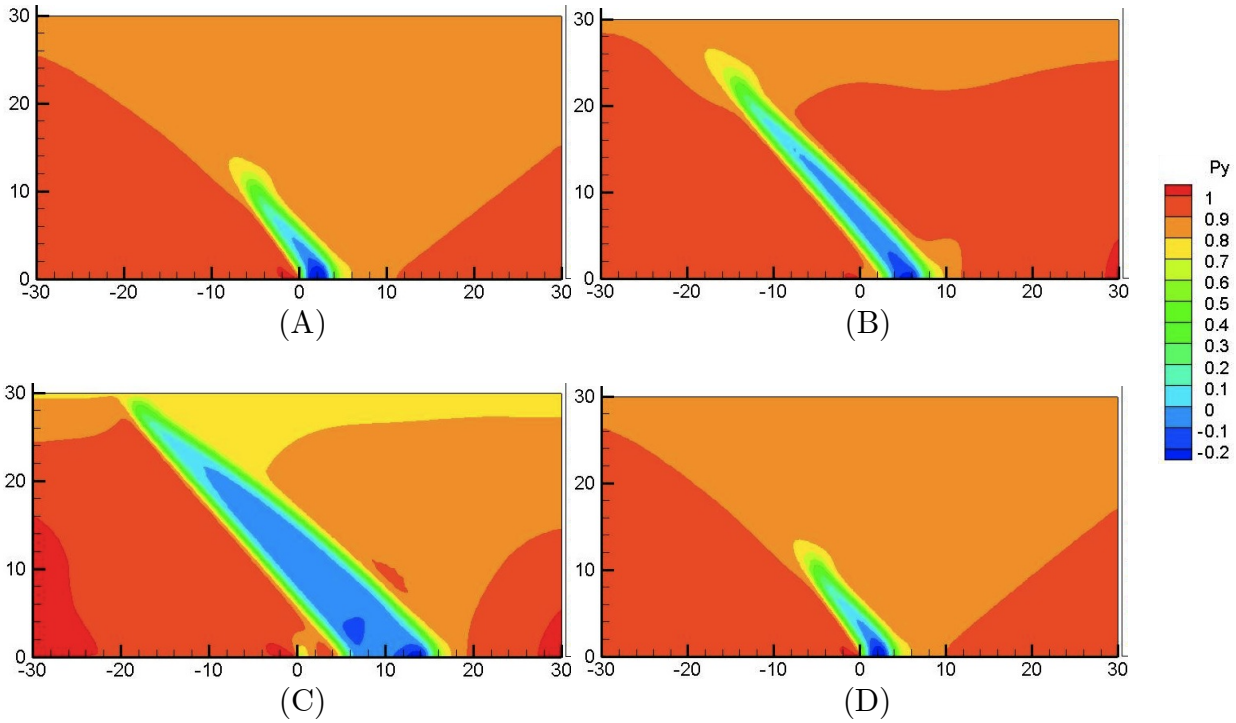

Fig. 3. Contour plots of the y component of the polarization normalized by P_0 in the vicinity of the crack tip for (A) $\omega_A / P_0 = 0.16$ during the non-equilibrium evolution of the domain, (B) $\omega_A / P_0 = 0.16$ at the final equilibrium state for the domain, (C) equilibrium at $\omega_A / P_0 = 0.2$, and (D) equilibrium at $\omega_A / P_0 = 0.11$. Only the upper half of the region is displayed. The x and y distances are normalized distances x / l_0 and y / l_0, and the polarization scale is normalized by the spontaneous polarization P_0.

Next, results for the apparent crack tip energy release rate calculation are presented. Figure 4a plots the apparent energy release rate as a function of the applied charge loading for the sample. Note that points A-D on Figure 4a correspond to the domain structures illustrated in Figures 3A-3D respectively. Initially, as the charge is applied the energy release rate is negative and approximately quadratic in the applied charge. These features of the energy release rate are in accord with linear piezoelectric fracture mechanics solutions. Furthermore, prior to the nucleation of the new domain, the solutions are carried out at equilibrium and the energy release rate calculation is path-independent. At the charge load level of $\omega_A / P_0 = 0.16$, nucleation of the new domain occurs, and at this point the crack tip energy release rate is approximately $\mathcal{G} = -3E_0 P_0 l_0$. The charge is held fixed at this point and as the new domain grows the energy release rate increases from $\mathcal{G} = -3E_0 P_0 l_0$ to $\mathcal{G} = 0.5E_0 P_0 l_0$.

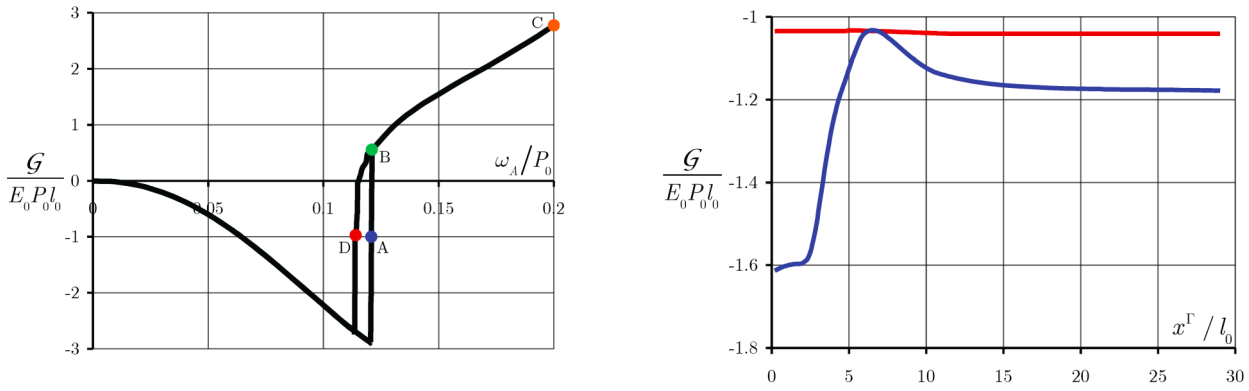

(a) (b)

Fig. 4. (a) The crack tip energy release rate as a function of the applied charge. Points A-D correspond to the domain structures illustrated in Figures 3A-3D respectively. (b) The apparent energy release rate for domain structures A (blue, non-equilibrium) and D (red, equilibrium).

Note that the domain evolution at $\omega_A / P_0 = 0.16$ is a non-equilibrium process during which the apparent energy release rate calculation is path-dependent. Specifically, path-dependence of the apparent energy release rate calculation for domain structure A is plotted as the blue curve in Figure 4b. Domain structure B is again an equilibrium configuration and the energy release rate calculation is path-independent. After domain structure B stabilizes, additional charge is applied and the domain structure is allowed to evolve at equilibrium to domain structure C. During this loading process the energy release rate increases in an approximately linear fashion. Upon reaching structure C the applied charge is removed and the domain structures and the energy release rate "unloads" along its original loading path to structure B. At this point the unloading path diverges from the original loading path and a hysteresis appears in the energy release rate versus applied charge response. Domain structure D is arrived at during the equilibrium unloading process and the energy release rate calculation is path-independent as shown by the red curve in Figure 4b. Further unloading of the charge causes the domain to vanish and the original negative quadratic branch of the energy release rate response is followed.

The most interesting aspect of this simulation is the departure from the results of linear piezoelectric fracture mechanics. Specifically, this calculation is the first that we are aware of that predicts that the crack tip energy release rate can be positive under purely electrical loading for impermeable crack face boundary conditions. Furthermore, the calculation shows that an existing domain structure near the crack tip can cause a qualitatively different behavior for the energy release rate, positive and increasing with applied charge, from what is expected in linear piezoelectricity, negative and decreasing with applied charge. We do note that *large scale switching* does occur in this simulation and so a direct comparison to linear piezoelectric fracture mechanics concepts is

tenuous. However, these simulations demonstrate the effects that near tip domain structures can have on the fracture process in ferroelectric crystals. Specifically, the negative contribution of the energy release rate from applied electric fields may in fact be positive for certain domain structures near crack tips. Hence, the modeling of crack tip domain structures and large scale domain switching behavior in fracture specimens may be a key to understanding the plethora of seemingly disparate experimental observations on electromechanical fracture of ferroelectrics.

Infinite Boundary Conditions for Crack Problems

During our studies of the switching zones near crack tips we found the need to develop infinite boundary conditions for two-dimensional crack being loaded by a K-field. To accomplish this we formulated a coupled analytic/finite-element method for two-dimensional crack problems. With the method two classes of problems can be studied. The first considers problems where non-linear constitutive processes occur in a region near the crack tip and the remotely applied loading can be characterized by the linear elastic K-field and perhaps the T-stress. In this case, the finite-element method is applied in a circular region around the crack tip where non-linear constitutive response is occurring, and stiffness contributions associated with a numerically implemented Dirichlet-to-Neumann map are imposed on the circular boundary to account for the large surrounding elastic domain and the remote applied loading. This is the class of problems relevant to the study of switching zones. The second class of problems considers entirely linear elastic domains with irregular external boundaries and/or complex applied loadings. Here, the discrete Dirichlet-to-Neumann map is used to represent a circular region surrounding the crack tip, and finite-elements are used for the external region. In this case the mixed mode stress intensity factors and the T-stress are retrieved from the map. This application of the method results in a highly accurate set of "crack-tip" elements that can be used to decompose the stress intensity factors from the T-stress in linear elastic (or linear piezoelectric) fracture mechanics problems. Full details of the method can be found in Reference [4].

Path-Dependence of the *J*-Integral

While this study seems somewhat tangential to the originally proposed work, it arose from our interests in how the ferroelastic switching zones near cracks in ferroelectrics affect the crack tip energy release rate. The section just prior to this one describes our work on the numerical implementation of the true small-scale yielding/switching boundary conditions for such crack problems. Our first test of the method was simply to look at the path-dependence of the J-integral in a standard elastic-plastic material governed by J_2-flow plasticity theory. The existing body of decades old literature on the topic suggested that the J-integral should be nearly but not exactly path-independent. What we found in this study was interestingly different and is shown in Figure 5.

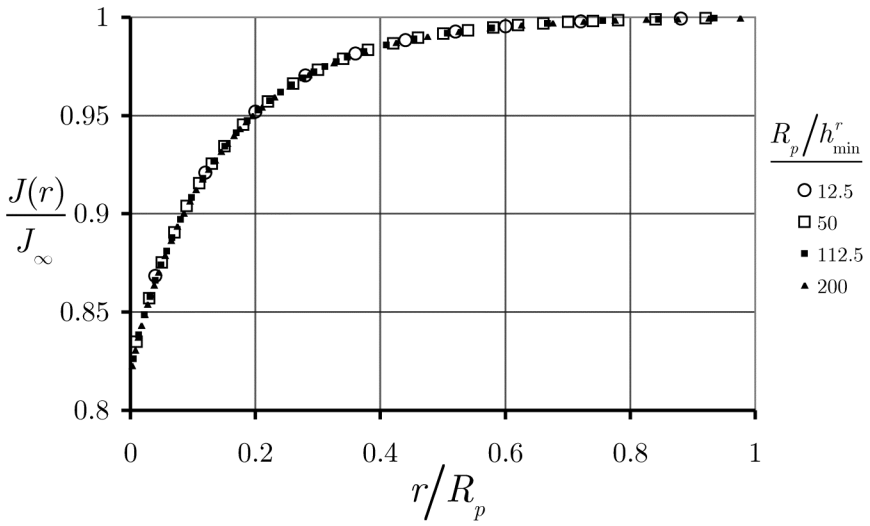

Fig. 5. Values for the J-integral normalized by its far-field value for a circular contour of radius r computed by the domain integral method near a crack tip under mode I loading in an elastic-perfectly-plastic material with $\nu = 0.3$. The markers correspond to different points along the load history and different sizes of the plastic zone relative to the minimum radial dimension of the elements surrounding the crack tip. R_p is the approximate plastic zone size and $h^r_{\min}$ is the minimum element size near the crack tip.

The results shown in Figure 5 indicate that there is significant, ~20%, path-dependence of the J-integral as the radius of the integration path is reduced. Additional details of this study can be found in Reference [5]. From an informal poll we determined that several experts in the area of elastic-plastic fracture mechanics found this results to be surprising. Hence, this work was able to fill a gap in the existing literature on the path-dependence of J in elastic-plastic materials. Continuing work in progress on J in ferroelastic materials has shown that J can actually be elevated at the crack tip due to ferroelastic switching.

Bibliography

1. Su Y, Landis CM. Continuum thermodynamics of ferroelectric domain evolution: Theory, finite element implementation and application to domain wall pinnin. J Mech Phys Solids 2007;55:280-305.

2. Kontsos A, Landis CM. Computational modeling of domain wall Interactions with dislocations in ferroelectric crystals. Int J Solids Struct 2009;46: 1491-8.

3. Li W, Landis CM. Nucleation and growth of domains near crack tips in single crystal ferroelectrics. Engrg Fract Mech 2010, accepted for publication.

4. Carka D, Mear ME, Landis CM. The Dirichlet-to-Neumann map for two-dimensional crack problems", in press Comp Meth Appl Mech Engrg (2011).

5. Carka D, Landis CM. On the path-dependence of the *J*-integral in an elastic-plastic material. J Appl Mech 2010;78: 011006.

Appendix

Equation (11) presented the general form of the Helmholtz free energy used in this paper. For a coordinate system aligned with the ⟨100⟩ directions, the specific form used to fit the dielectric, piezoelectric and elastic properties of ferroelectric single crystals that undergo a cubic to tetragonal phase transformation is given in Equation (A1).

$$
\begin{aligned}
\psi = {} & \frac{a_0}{2}\left(P_{1,1}^2 + P_{2,2}^2 + P_{3,3}^2 + P_{1,2}^2 + P_{2,1}^2 + P_{1,3}^2 + P_{3,1}^2 + P_{2,3}^2 + P_{3,2}^2\right) \\
& + \frac{a_1}{2}\left(P_1^2 + P_2^2 + P_3^2\right) + \frac{a_2}{4}\left(P_1^4 + P_2^4 + P_3^4\right) + \frac{a_3}{2}\left(P_1^2P_2^2 + P_2^2P_3^2 + P_1^2P_3^2\right) \\
& + \frac{a_4}{6}\left(P_1^6 + P_2^6 + P_3^6\right) + a_6\left(P_1^4(P_2^2 + P_3^2) + P_2^4(P_1^2 + P_3^2) + P_3^4(P_1^2 + P_2^2)\right) \\
& + \frac{a_5}{4}\left(P_1^4P_2^4 + P_2^4P_3^4 + P_1^4P_3^4\right) \\
& - \frac{b_1}{2}\left(\varepsilon_{11}P_1^2 + \varepsilon_{22}P_2^2 + \varepsilon_{33}P_3^2\right) - \frac{b_2}{2}\left((\varepsilon_{22} + \varepsilon_{33})P_1^2 + (\varepsilon_{11} + \varepsilon_{33})P_2^2 + (\varepsilon_{11} + \varepsilon_{22})P_3^2\right) \\
& - b_3\left((\varepsilon_{12} + \varepsilon_{21})P_1P_2 + (\varepsilon_{13} + \varepsilon_{31})P_1P_3 + (\varepsilon_{23} + \varepsilon_{32})P_2P_3\right) \\
& + \frac{c_1}{2}\left(\varepsilon_{11}^2 + \varepsilon_{22}^2 + \varepsilon_{33}^2\right) + c_2\left(\varepsilon_{11}\varepsilon_{22} + \varepsilon_{11}\varepsilon_{33} + \varepsilon_{22}\varepsilon_{33}\right) + \frac{c_3}{2}\left(\left(\varepsilon_{12} + \varepsilon_{21}\right)^2 + \left(\varepsilon_{13} + \varepsilon_{31}\right)^2 + \left(\varepsilon_{23} + \varepsilon_{32}\right)^2\right) \\
& + \left(\frac{f_1}{2}\varepsilon_{11}^2 + \frac{f_2}{2}(\varepsilon_{22}^2 + \varepsilon_{33}^2) + f_3(\varepsilon_{11}\varepsilon_{22} + \varepsilon_{11}\varepsilon_{33}) + f_4\varepsilon_{22}\varepsilon_{33} + \frac{f_5}{2}\left(\left(\varepsilon_{12} + \varepsilon_{21}\right)^2 + \left(\varepsilon_{13} + \varepsilon_{31}\right)^2\right) + \frac{f_6}{2}\left(\varepsilon_{23} + \varepsilon_{32}\right)^2\right)P_1^2 \\
& + \left(\frac{f_1}{2}\varepsilon_{22}^2 + \frac{f_2}{2}(\varepsilon_{11}^2 + \varepsilon_{33}^2) + f_3(\varepsilon_{11}\varepsilon_{22} + \varepsilon_{22}\varepsilon_{33}) + f_4\varepsilon_{11}\varepsilon_{33} + \frac{f_5}{2}\left(\left(\varepsilon_{12} + \varepsilon_{21}\right)^2 + \left(\varepsilon_{23} + \varepsilon_{32}\right)^2\right) + \frac{f_6}{2}\left(\varepsilon_{13} + \varepsilon_{31}\right)^2\right)P_2^2 \\
& + \left(\frac{f_1}{2}\varepsilon_{33}^2 + \frac{f_2}{2}(\varepsilon_{11}^2 + \varepsilon_{22}^2) + f_3(\varepsilon_{11}\varepsilon_{33} + \varepsilon_{22}\varepsilon_{33}) + f_4\varepsilon_{11}\varepsilon_{22} + \frac{f_5}{2}\left(\left(\varepsilon_{13} + \varepsilon_{31}\right)^2 + \left(\varepsilon_{23} + \varepsilon_{32}\right)^2\right) + \frac{f_6}{2}\left(\varepsilon_{12} + \varepsilon_{21}\right)^2\right)P_3^2 \\
& + \left(\frac{g_1}{4}\varepsilon_{11} + \frac{g_2}{4}(\varepsilon_{22} + \varepsilon_{33})\right)P_1^4 + \left(\frac{g_1}{4}\varepsilon_{22} + \frac{g_2}{4}(\varepsilon_{11} + \varepsilon_{33})\right)P_2^4 + \left(\frac{g_1}{4}\varepsilon_{33} + \frac{g_2}{4}(\varepsilon_{11} + \varepsilon_{22})\right)P_3^4 \\
& + \frac{g_3}{4}\left(\varepsilon_{12} + \varepsilon_{21}\right)\left(P_1P_2^3 + P_2P_1^3\right) + \frac{g_3}{4}\left(\varepsilon_{13} + \varepsilon_{31}\right)\left(P_1P_3^3 + P_3P_1^3\right) + \frac{g_3}{4}\left(\varepsilon_{23} + \varepsilon_{32}\right)\left(P_2P_3^3 + P_3P_2^3\right) \\
& + \frac{1}{2\kappa_0}\left((D_1 - P_1)^2 + (D_2 - P_2)^2 + (D_3 - P_3)^2\right)
\end{aligned}
\tag{A1}
$$

In the equation above $\kappa_0 = 8.854 \times 10^{-12}$ Vm/C, and

$$
\begin{aligned}
a_1 &= -0.668325\, E_0/P_0 & a_2 &= -3.80653\, E_0/P_0^3 & a_3 &= 0.78922\, E_0/P_0^3 \\
a_4 &= 12.4421\, E_0/P_0^5 & a_6 &= 0.134226\, E_0/P_0^5 & & \\
b_1 &= 2.54138\, E_0/\varepsilon_0 P_0 & b_2 &= 1.74267\, E_0/\varepsilon_0 P_0 & b_3 &= 0.399353\, E_0/\varepsilon_0 P_0 \\
c_1 &= 2.04999\, \sigma_0/\varepsilon_0 & c_2 &= 0.971673\, \sigma_0/\varepsilon_0 & c_3 &= 1.27976\, \sigma_0/\varepsilon_0 \\
f_1 &= 0.663581\, E_0/\varepsilon_0^2\, P_0 & f_2 &= 0.841326\, E_0/\varepsilon_0^2\, P_0 & f_3 &= -0.170635\, E_0/\varepsilon_0^2\, P_0 \\
f_4 &= 0.687281\, E_0/\varepsilon_0^2\, P_0 & f_5 &= 0.106647\, E_0/\varepsilon_0^2\, P_0 & f_6 &= 0.213294\, E_0/\varepsilon_0^2\, P_0
\end{aligned}
$$

$$g_1 = -3.66149\, E_0 \big/ \varepsilon_0 P_0^3 \qquad g_2 = 6.27423\, E_0 \big/ \varepsilon_0 P_0^3 \qquad g_3 = -1.21644\, E_0 \big/ \varepsilon_0 P_0^3$$

where $\sigma_0 = E_0 P_0 / \varepsilon_0 = 692 \times 10^6$ N/m^2. In addition, $P_0 = 0.26$ C/m^2, $\varepsilon_0 = 0.0082$ and $E_0 = 2.182 \times 10^7$ V/m correspond to properties of monodomain single crystal barium titanate at room temperature.

The parameter a_0 appearing in Eq. (A1) determines the domain wall thickness. If $a_0 = 1 \times 10^{-10}$ V$\cdot$m^3 / C $a_o =$ then $l_0 = 1$ nm, and therefore the 180° domain wall has thickness equal to 2 nm which is in general agreement with experimental observations.